



Earth and Space Science

RESEARCH ARTICLE

10.1029/2021EA001857

Detection and Attribution of Norwegian Annual Precipitation Variability Related to Teleconnections

Yanlai Zhou^{1,2} , Gusong Ruan³, Chong-Yu Xu¹ , Lihua Xiong², Sharad K. Jain⁴, and Lu Li⁵

¹Department of Geosciences, University of Oslo, Oslo, Norway, ²State Key Laboratory of Water Resources and Hydropower Engineering Science, Wuhan University, Wuhan, China, ³Norwegian Water Resources and Energy Directorate (NVE), Oslo, Norway, ⁴Indian Institute of Technology, Roorkee, India, ⁵Bjerknes Centre for Climate Research, NORCE Norwegian Research Centre, Bergen, Norway

Key Points:

- Significant abrupt changes, increases and periodicities (40–50 years) constitute the Norwegian annual precipitation variability
- The maximal information coefficient adequately associates the Norwegian precipitation variability with teleconnections
- The maximal information coefficient captures hook structures of relationships between precipitation and teleconnections

Correspondence to:

Y. Zhou and C.-Y. Xu,
yanlai.zhou@whu.edu.cn;
c.y.xu@geo.uio.no

Citation:

Zhou, Y., Ruan, G., Xu, C.-Y., Xiong, L., Jain, S. K., & Li, L. (2022). Detection and attribution of Norwegian annual precipitation variability related to teleconnections. *Earth and Space Science*, 9, e2021EA001857. <https://doi.org/10.1029/2021EA001857>

Received 18 MAY 2021

Accepted 13 JAN 2022

Author Contributions:

Conceptualization: Gusong Ruan, Sharad K. Jain, Lu Li
Data curation: Yanlai Zhou, Gusong Ruan
Formal analysis: Yanlai Zhou, Chong-Yu Xu, Lu Li
Funding acquisition: Chong-Yu Xu, Lihua Xiong
Investigation: Yanlai Zhou, Chong-Yu Xu, Lihua Xiong, Sharad K. Jain, Lu Li
Methodology: Yanlai Zhou, Gusong Ruan, Chong-Yu Xu, Lihua Xiong, Sharad K. Jain

Abstract Detection and attribution of precipitation variability are fundamentally challenging, especially in the presence of complex nonlinear relationships between precipitation variability and large-scale teleconnections. The aim of this study is twofold. First, we identify abrupt changes and the trend and periodicity characteristics of long-term (1950–2019) annual precipitation series over the Norway mainland by using the Multiple Comparison Procedures, the Mann-Kendall test, and the Wavelet Analysis. Second, we interpret the variability characteristics found over five regions of Norway by exploring their relationships with teleconnections through the Maximal Information Coefficient. The results indicate that significant abrupt changes appeared in the mean (variance) value of annual precipitation series at 117 (49) out of 159 rainfall stations of five regions in Norway at a significance level of 0.05. The occurrences of change points varied from 1979 to 1984 in five regions of Norway. The mean and variance of the annual precipitation series increased by 32% and 16% at most, respectively, compared with those values before the change points. The first periodicity (spanning four to five decades) was the dominant periodic component and could be used to best characterize the Norwegian precipitation variability. Because the subtropical Azores High (subpolar Icelandic Low) moves toward (away from) Europe, the relationship between the annual precipitation series and the Scandinavian pattern (Atlantic Multidecadal Oscillation) series tended to be of an upward (downward) hook structure. The association of precipitation variability and teleconnections found in this study can pave the way for new possibilities with regard to detection and attribution of precipitation variability.

1. Introduction

Long-term planning and management of water resources, multisector water demand and supply as well as related infrastructures are closely associated with the capability and reliability of characterizing variations in precipitation (Sun et al., 2018). The first task is to characterize the statistics of precipitation data by using the long-term reliable observed precipitation series. To implement statistical analysis, a stationarity assumption is usually made for relevant time series. According to Salas (1993), “A time series is stationary when it is free of change points, trends or periodicities.” However, the stationarity assumption has been challenged by observations and modeling results recently (Lee & Ouara, 2010; Li et al., 2015; Montanari & Koutsoyiannis, 2014; Russo et al., 2013; Sang et al., 2016; Torres-Batló & Martí-Cardona, 2020). There is an increasing research interest in the detection and attribution analysis of the nonstationarity in hydro-climatic time series (e.g., Liu et al., 2020; Papalexou & Montanari, 2019).

For Norway and even the whole of Europe, abrupt changes, trend and periodicity characteristics in climatic and hydrological time series have been widely discussed in the past (Dyrddal et al., 2012, 2015; Førland & Kristoffersen, 1989; Vicente-Serrano & López-Moreno, 2008; Zveryaev, 2006). Ingebrigtsen et al. (2014, 2015) adopted a spatial approach for modeling the nonstationarity of the regional annual precipitation time series in southern Norway. Blanchet et al. (2015) detected an increasing trend of extreme precipitation in the southwestern part of Norway by using the output of a probabilistic rainfall estimation model. Dyrddal et al. (2016) investigated the spatial variability of extreme precipitation and estimated the variation in the shape parameter of the generalized extreme value distribution of extreme areal precipitation in Norway by using a gridded data set. Cieszyńska and Stramska (2018) revealed the statistically significant trends of annual air temperature and a noticeable spatial variability of the meteorological conditions in the Porsanger fjord of Norway. Dyrddal et al. (2018) evaluated the trend of subdaily and daily summer precipitation in Norway based on gridded datasets and found that summer extreme

© 2022 The Authors. Earth and Space Science published by Wiley Periodicals LLC on behalf of American Geophysical Union.

This is an open access article under the terms of the [Creative Commons Attribution-NonCommercial-NoDerivs License](https://creativecommons.org/licenses/by-nc-nd/4.0/), which permits use and distribution in any medium, provided the original work is properly cited, the use is non-commercial and no modifications or adaptations are made.

Project Administration: Chong-Yu Xu, Lihua Xiong
Resources: Gusong Ruan, Chong-Yu Xu
Software: Yanlai Zhou, Lu Li
Supervision: Gusong Ruan, Chong-Yu Xu
Validation: Gusong Ruan, Lihua Xiong, Sharad K. Jain, Lu Li
Visualization: Yanlai Zhou
Writing – original draft: Yanlai Zhou
Writing – review & editing: Gusong Ruan, Chong-Yu Xu, Lihua Xiong, Sharad K. Jain, Lu Li

precipitation displays significant spatial variability in association with the complex topography and low-pressure systems in the North Atlantic. Skogseth et al. (2020) evaluated the trends in the Isfjorden fjord's climate and circulation and attributed the cause of the shift of Atlantic water to positive trends in mean air temperature and mean sea surface temperature of the European Arctic by combining observational and reanalysis datasets. Trend analysis, the most frequently used approach, can adequately extract the strong or dominant global trends from time series. The comprehensive analysis of abrupt change, trend and periodicity would facilitate the description of the variability in global and local processes, especially concerning some local variable characteristics hidden in the strong or dominant global trends of the time series. Although extra efforts are required to comprehensively detect each possible variability, additional information acquired is highly useful to improve the understanding of global and local variable characteristics and how these three characteristics interact with each other. Therefore, it would be interesting and important to conduct the comprehensive research from the perspectives of abrupt change, trend, and periodicity analysis for improving the understanding of precipitation variability detection.

Furthermore, the attribution analysis of nonstationarity in hydro-meteorological time series has become increasingly important (Guo et al., 2020; Lee et al., 2019; Pei, et al., 2018; Sarojini, et al., 2016). Understanding precipitation variability as well as its association with teleconnections is beneficial for a better adaptation to varying climatic conditions and a reduction in the damage related to climate change. The annual and interannual-to-decadal teleconnections (or oscillations) are often regarded as two of the most notable patterns and explanatory variables of climatic and hydrological variability (e.g., Hua et al., 2019; Lee et al., 2018; Li et al., 2018; Murgulet et al., 2017; Yin & Zhou, 2018). Valdés-Pineda et al. (2018) adopted Singular Spectrum Analysis techniques to analyze the combined influence of two teleconnections on the variability of monthly precipitation in Chile. Mayta et al. (2019) combined the principal component analysis and the empirical orthogonal function for quantifying the impact of Madden-Julian oscillation on intraseasonal precipitation variability in the Amazon catchment. Furthermore, Börgel et al. (2020) argued that both Atlantic Multidecadal and North Atlantic oscillations have a prominent influence on the North European climate variability, which partially confirms the results obtained by Asong et al. (2018) and Nalley et al. (2019). Besides, plenty of studies have made contributions to attribution analysis of hydro-meteorological variability. Most of these researches have centered on modeling the linear relationship between trend characteristics and oscillations. Hence, a better exploration of the complex relationship between teleconnections and precipitation is required to feature precipitation variability.

From the perspective of Norwegian climatic variability detection, previous researches primarily concentrated on global trend analysis. From the perspective of the physical-cause analysis of climatic variability, many fundamental challenges still exist in variability attribution analysis, whereas little attention was paid to the capture of the complex nonlinear relationships between teleconnections and precipitation.

The purpose of this study is twofold. First, we detect the variability of long-term annual precipitation series in Norway by applying a comprehensive variability detection approach. Second, we associate annual and interannual-to-decadal teleconnection indices with annual precipitation series by introducing the Maximal Information Coefficient (MIC) to explain such climatic variability.

The rest of this manuscript is structured as follows. We describe the study area and materials in Section 2 and the methods adopted in Section 3. The methods adopted to perform the detection and attribution analysis of annual precipitation variability and the discussion of results are presented in Section 4. The main findings and conclusions are summarized in Section 5.

2. Study Area and Materials

2.1. Study Area

Norway (Figure 1) is located in the western part of the Northern Europe and has a total administrative area of 385,251 km² (our study area occupying 324,220 km² covers the mainland Norway, excluding the Svalbard and Jan Mayen). Due to a large span of latitude and varied topography, the meteorological conditions in the country display a high spatial variability. The average annual precipitation varies from around 600 mm in northeastern and central-eastern areas to over 3,000 mm in the southwestern area. The precipitation volume is commonly influenced by various Northern Hemisphere atmospheric processes and reaches peaks during autumn and winter, except the eastern Norway which exhibits cold-dry winter and the maximal precipitation volumes often occur in summer (Yan et al., 2019). Extreme precipitation and flooding have large social costs in Norway, hence, accurate

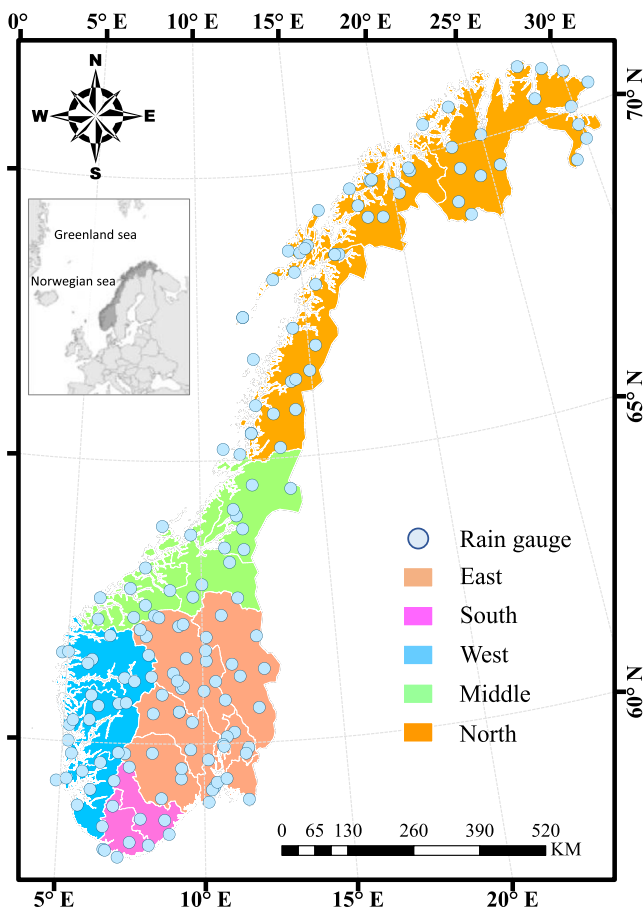


Figure 1. Study area and locations of the selected 159 rainfall monitoring stations in five regions over the whole Norway mainland.

implementation of detection and attribution analysis on precipitation series would allow for a better adaptation to varying climatic conditions and a reduction in the damage caused by climate change.

2.2. Materials

In Norway, three types of surface rain gauges are employed to measure precipitation. Regular monitoring stations measure precipitation by a simple manually operated bucket, and the total precipitation volume is often recorded once a day. Automated monitoring stations hold either weight pluviometer or tipping bucket facilities. More details on precipitation measurements and data quality control can be found in the data policy released by the Meteorological Institute (MET) of Norway (<https://www.met.no/>).

The Norwegian meteorological network that monitors daily precipitation contains more than 550 stations in 2019, about 200 of which also gauge hourly rainfall. Significant variation in the number of monitoring stations appeared over the years, leading to rare long-term precipitation observations for a common study period. Because most of the gauges have been installed at lower elevations in southwestern Norway, the spatial distribution of the gauges is slightly inhomogeneous. Consequently, data of 159 rainfall stations are used to detect and attribute the variability of long-term annual precipitation series owing to the following reasons: (a) The length of the precipitation data set at each station is larger than 30 years while the continuous data length varies from 31 to 70 years (1950–2019); (b) the stations are evenly distributed in five regions of Norway (Hegdahl et al., 2019). A total of 22 out of 159 stations have samples close to 70 and 91 out of 159 stations have samples close to 50. The location of Norway and 159 precipitation monitoring stations is illustrated in Figure 1. The numbers of precipitation stations in five regions are: 49 (East), 11 (South), 24 (West), 22 (Middle), and 53 (North), respectively.

Teleconnections refer to the associations of atmospheric and oceanic climate system anomalies that occur over long distances. Several Northern Hemisphere teleconnection patterns have been considered in this study to identify their associations with nonstationary annual precipitation series over Norway mainland, including (annual oscillations) the Scandinavian pattern (SCAND), the North Atlantic Oscillation (NAO) and the East Atlantic/Western Russia pattern (EAWR) as well as (interannual-to-decadal oscillations) the Atlantic Multidecadal Oscillation (AMO) and the Madden-Julian Oscillation (MJO). These teleconnection patterns have been associated in the literature not only with common meteorological variables such as precipitation and temperature, but also with streamflow, snow cover, or crop production (e.g., Delworth & Zeng, 2016; Irannezhad et al., 2020; Mahajan et al., 2018; Wu & Hu, 2015).

Precipitation data of 159 gauge stations were extracted from various sources: the Global Summary of the Day (GSOD) datasets are accessible on the website of the National Climate Data Center (<https://catalog.data.gov/dataset/global-surface-summary-of-the-day-gsod>); the North Atlantic Oscillation (NAO), the East Atlantic/Western Russia pattern (EAWR) and the Atlantic Multidecadal Oscillation (AMO) are accessible on the website of the National Oceanic and Atmospheric Administration (<https://psl.noaa.gov/data/climateindices/list/>); the Scandinavian pattern (SCAND) is accessible on the website (<https://www.cpc.ncep.noaa.gov/data/teledoc/telecontents.shtml>); and the Madden-Julian Oscillation (MJO) is accessible on the website (https://www.cpc.ncep.noaa.gov/products/precip/CWlink/mjo_iso.html). The annual teleconnection indices have a spatial resolution of $1^\circ \times 1^\circ$ from 1950 to 2019.

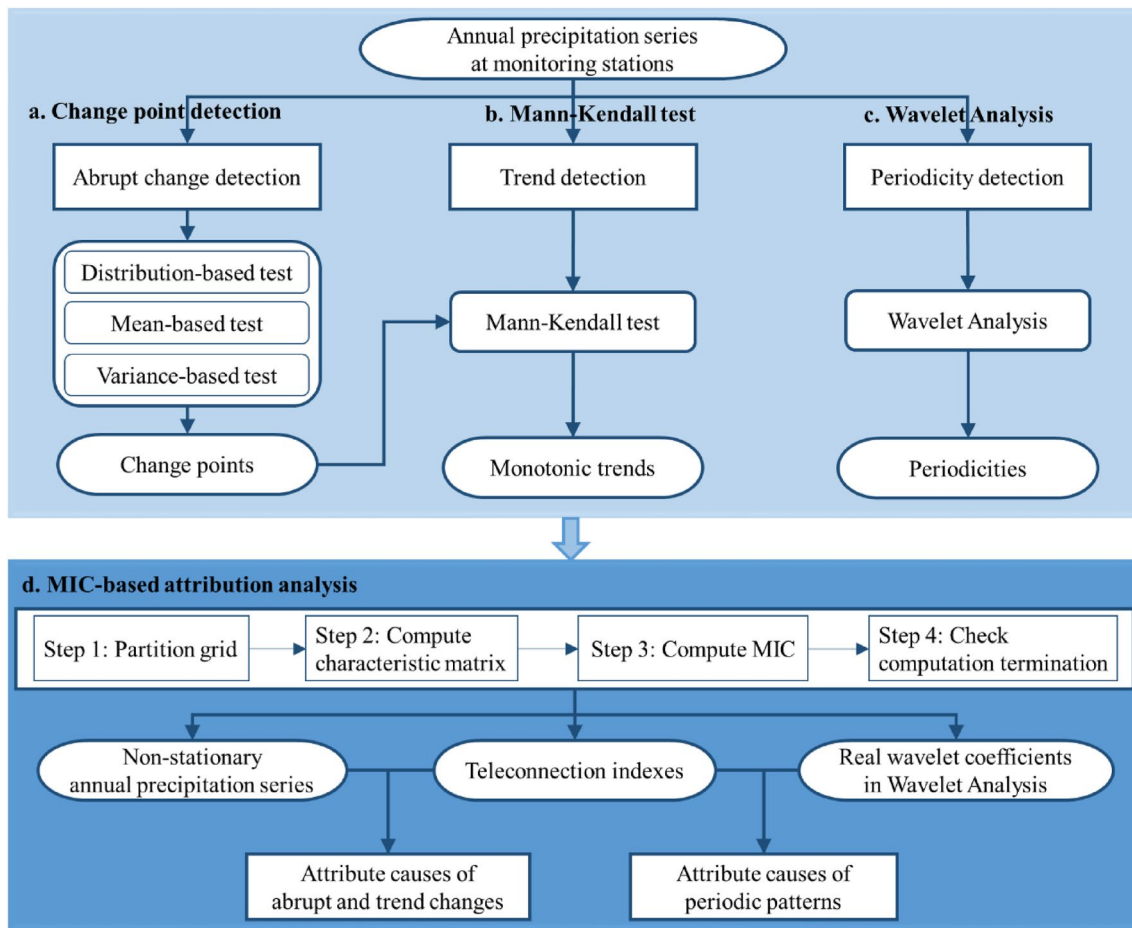


Figure 2. Main analytical architectures adopted in this study. (a) Change point detection approach. (b) Mann-Kendall test. (c) Wavelet Analysis. (d) Maximal Information Coefficient (MIC)-based attribution analysis.

3. Methods

Figure 2 illustrates the analysis flowchart adopted in this study. The analysis consists of the following components: the multiple comparison procedures for change point detection (Figure 2a); the Mann-Kendall test for trend detection (Figure 2b); the Wavelet Analysis for periodicity detection (Figure 2c); and the Maximal Information Coefficient-based attribution analysis (Figure 2d).

3.1. Nonstationarity Detection

The aim of this section is to identify and test the statistical significance of change points, trends, and periodicities in time series. The related detection methods are described as follows.

3.1.1. Multiple Comparison Procedures for Change Point Detection

Gradual long-term climate change differs from abrupt climate change. More attention has been paid in the literature and IPCC reports on the gradual climate change over many decades or even longer. Abrupt climate change occurs in a matter of years or a few decades and has probably made a greater impact upon both human societies and natural environments than gradual climate change. For example, severe droughts and extremely high temperature events are the most serious abrupt climate change events (Wathen, 2011). The physical reason for abrupt discharge change can be attributed to precipitation change, land use change and flow regulation of rivers; however, causes of abrupt climate changes are far from clear. The abrupt change in temperature and precipitation might have associations with regional atmospheric circulation, and besides, solar variability. Volcanic activities, tropospheric aerosols, and increase in concentration of greenhouse gases, among other factors, are also believed

Table 1
Three Types of Change Detection Methods Adopted in This Study

| Method | Detected year: End ^a or start ^b | Detection type | Single or multiple change points |
|--------------------|---|--------------------|----------------------------------|
| Pettitt | Start | Mean based | Single |
| Mann-Whitney | End | Mean based | Multiple |
| Lombard Mood | End | Variance based | Single |
| Mood | End | Variance based | Multiple |
| Anderson Darling | End | Distribution based | Single |
| Kolmogorov-Smirnov | End | Distribution-based | Multiple |
| Cramer-von Mises | End | Distribution based | Multiple |

^aEnd refers to the end year of a previous homogeneous subset. ^bStart refers to the start year of a subsequent homogeneous subset.

to cause changes, though no clear lines of evidence have been developed (Chen et al., 2014; Temnerud & Weyhenmeyer, 2008).

In general, the change point detection concentrates on the parameters of location (mean or the first moment) and scale (variance or the second moment), whereas the shape parameter (the third moment) is assumed to be constant with time for achieving model stability and applicability (Cannon, 2010; Zhou, 2020). Note that methods that only detect differences in the mean will not detect nonstationarities present in other moments. The same argument applies to methods for detecting nonstationarity in variance and shape parameter. For this reason, this study recruits several methods that assess nonstationarities in time series datasets driven by changes in the mean and variance, as well as in the distributional properties of the data set (Table 1). These methods include the Pettitt and Mann-Whitney method for testing changes in mean values, the Lombard Mood and Mood methods for detecting changes in variance, and the Anderson Darling, Kolmogorov-Smirnov and Cramer-Von-Mises methods for assessing the changes in the underlying distribution. More details on the Kolmogorov-Smirnov, Cramer-von Mises, Pettitt, Mann-Whitney, Lombard Mood and Mood tests can be found in Erdman and Emerson (2007), Ross (2015), James and Matteson (2015), and Friedman et al. (2016).

3.1.2. Mann-Kendall Test for Trend Detection

As mentioned earlier, abrupt change and gradual trend change are two different forms of nonstationarity and have different causes and physical reasons. But both can exist simultaneously in the observed data series. Abrupt change detection is conducted prior to the trend analysis of subdivided series. Subdivided series may or may not have trends in mean and variance. That is to say if change-points in mean/variance are detected, the subset timeseries may not necessarily be stationary in the mean/variance. These may have different trends that are either significant or insignificant (equivalent to no trend). Consequently, a trend test is required to check if there are monotonic trends in the subset and entire timeseries.

Mann (1945) formulated the Mann-Kendall test as a nonparametric test for trend detection while Kendall (1975) further derived the statistical distribution of the test for identifying nonlinear trends. The test has been widely employed to identify trends in hydro-meteorological time series (e.g., Ahmad et al., 2015; Júnior et al., 2020). However, the positive or negative autocorrelation in a time series would affect the trend test statistics (Yue & Wang, 2002). Hence, the prewhitening-based (Bayazit & Önöz, 2007) Mann-Kendall test was employed to detect monotonic trends of annual precipitation series in the subsets or the entire set of the data in this study. The description of the prewhitening-based Mann-Kendall test is given in Appendix A.

3.1.3. Wavelet Analysis for Periodicity Detection

Wavelet Analysis is an effective approach to detecting the periodicity of nonstationary time series since it is able to provide harmonious localization of the temporal-frequency resolution in comparison to Fourier Transform and Semivariance Analysis (El-Borie et al., 2020; Song et al., 2018; Tan et al., 2016). The general form of the Wavelet Analysis function is described below.

$$\psi(a, b) = a^{-1/2} \cdot \psi\left(\frac{t-b}{a}\right) \quad (1)$$

where $\psi(a, b)$ is the wavelet basis function, and a and b are the scale and time shift parameters. The common wavelet basis function used in most hydro-meteorological applications is the Morlet wavelet (Baidu et al., 2017; Kang & Lin, 2007). The continuous Wavelet Analysis is calculated by the convolution of $x(t)$ time series with the wavelet base function $\psi(a, b)$.

Table 2
Comparison of Common Correlation Coefficients

| Correlation coefficient | Reference | Range | Cons | Pros (Applicability) |
|--------------------------|-----------------------|----------------|--|--|
| Pearson | Pearson (1895) | $[-1, 1]$ | Only for measuring linear correlation | Discrete variable with the same time interval or continuous variable |
| Spearman rank | Spearman (1904) | $[-1, 1]$ | Lower accuracy than Product-Moment | Ordered variables, not following normal distribution |
| Kendall rank | Kendall (1938) | $[-1, 1]$ | Requiring the rank sampling method | Ordered variables, not following normal distribution |
| Mutual information | Shannon (1948) | $[0, +\infty)$ | Difficult to calculate and without normalization | No assumption for marginal distributions |
| Correlation of distances | Székely et al. (2007) | $[0, 1]$ | Independent correlation with a positive value | Good generalizability with calculated Euclidean distance |
| MIC | Reshef et al. (2011) | $[0, 1]$ | High computational complexity | Good generalizability with normalization meanwhile measuring both linear and nonlinear correlation |

$$W(a, b) = a^{-1/2} \cdot \int_{-\infty}^{+\infty} f(t) \cdot \bar{\psi} \left(\frac{t-b}{a} \right) dt \quad (2)$$

where $W(a, b)$ is the continuous Wavelet Analysis function with parameters a and b . $\bar{\psi}(\cdot)$ is the complex conjugate function, and $f(t)$ is the continuous series over time t .

Since most hydro-meteorological time series are discrete, the continuous Wavelet Analysis function can be converted to a discrete one by a discrete scale representation.

$$W'(a, b) = a^{-1/2} \cdot \Delta t \cdot \sum_{p=1}^n f(p \cdot \Delta t) \cdot \bar{\psi} \left(\frac{p \cdot \Delta t - b}{a} \right) \quad (3)$$

where $W'(a, b)$ is the discrete Wavelet Analysis with parameters a and b . Δt is the time length of the discrete scale, and p and n are the index and numbers of data points, respectively.

To identify the periodicity of a time series, the wavelet variance is calculated by the convolution of the squared Wavelet Analysis over the time shift parameter b .

$$\text{Var}(a) = \int_{-\infty}^{+\infty} [W'(a, b)]^2 db \quad (4)$$

where $\text{Var}(a)$ is the wavelet variance. The plot of wavelet variance over the scale parameter (a) reveals the periodicities of a time series over various temporal-frequency resolutions. A periodicity with a large wavelet variance value implies it would be the dominant periodic component of a time series.

3.2. Maximal Information Coefficient (MIC)-Based Attribution Analysis

The MIC is regarded as a powerful method for quantifying the relationship between various variables, which measures the correlation coefficient in the range $[0, 1]$ (Reshef et al., 2011). The MIC can capture wide-ranging associations in both linear and nonlinear as well as both functional and nonfunctional aspects (Kinney & Atwal, 2014), compared to the correlation coefficients of Pearson, Spearman, Kendall, mutual information and correlation of distances (Table 2). Therefore, we calculated the MIC between teleconnection indices and annual precipitation series (wavelet coefficients) to perform attribution analysis on the variability (periodicity) in annual precipitation series.

The MIC is calculated on the basis of a distribution of two datasets (T, P), where T and P are two random variables (e.g., T is the teleconnection index and P is annual precipitation series). The application of MIC to attribution analysis for nonstationary annual precipitation series is described as follows.

Step 1. Partition grids and calculate mutual information of distribution. Given a dataset D with ordered pairs (T, P) , the x - and y -values of D can be partitioned into x columns and y rows, respectively. A pair of partitions refer to an x -by- y grid. For a grid G , we call $D|_G$ the distribution that is determined by the points in the dataset D on the cells of G . For a finite dataset D , different grids G lead to different distribution $D|_G$. Then, the mutual information can be calculated as follows.

$$I(D|_G) = \int dx dy f(x, y) \log_2 \left(\frac{f(x, y)}{f(x)f(y)} \right) \quad (5a)$$

$$I^*(D, x, y) = \max I(D|_G) \quad (5b)$$

where $I(D|_G)$ is the mutual information of distribution $D|_G$, $I^*(D, x, y)$ is the maximal mutual information over all grids G with x columns and y rows. $f(x)$ and $f(y)$ are the probability distribution functions of x - and y -values of D , respectively. $f(x, y)$ is the joint probability distribution function of the x - and y -values of D .

Step 2. Compute the characteristic matrix of D in terms of $I^*(D, x, y)$. For achieving stable convergence, this study implemented normalization by $\log_2 \min \{x, y\}$ for x columns and y rows to produce a score that can be compared over all grids with different dimensions and distributions. The infinite characteristic matrix $M(D, x, y)$ of a finite dataset D with x columns and y rows can be computed as follows.

$$M(D, x, y) = \frac{I^*(D, x, y)}{\log_2 \min \{x, y\}} \quad (6)$$

where $M(D, x, y)$ is the characteristic matrix of a finite data set D with x columns and y rows.

Step 3. Compute MIC in terms of $M(D, x, y)$ and grid size $B(n)$. The function $B(n)$ is the grid size varying with the sample size n , where $0 < B(n) \leq n^{1-\epsilon}$ ($0 < \epsilon < 1$) (Kinney & Atwal, 2014; Reshef et al., 2011). It is important to determine a suitable value for $B(n)$ because very large $B(n)$ can cause nonzero scores even for random variables while very small $B(n)$ implies the search is conducted only for simple patterns. In this study, we adopted $B(n) = n^{0.6}$, for which the value was determined through a trial-and-error procedure. Therefore, the MIC of a finite dataset D with ordered sample pairs (x, y) , sample size n and grid size less than $B(n)$ is calculated as follows.

$$\text{MIC}(D) = \max_{xy < B(n)} \{M(D, x, y)\} \quad (7)$$

where $\text{MIC}(D)$ is the maximal information coefficient of a finite data set D .

Step 4. Check whether the computation process terminates. Switch the grid over axes, repeat the above steps until the maximal value of information coefficients is obtained. The MIC value closer to 1 implies high correlation while closer to 0 suggests the variables are probably independent. It is clear that if the two random variables are independent, the joint distribution is the product of marginals and MIC tends to zero. Reshef et al. (2011) proved that noiseless functional relationships (i.e., Pearson correlation coefficient $R = 1.0$) receive an MIC value of about 1.0 if the two random variables are fully dependent.

4. Results and Discussion

Aiming at identifying and quantifying the nonstationary characteristics in long term annual precipitation series, the results for detecting change points, trend and periodicity as well as for attributing the causes of nonstationary characteristics are presented and discussed in Sections 4.1 and 4.2, respectively.

4.1. Detection of Nonstationarity in Annual Precipitation Series

First, the results of multiple methods at a significance level of 0.05 on the abrupt changes in the distribution, and the mean and variance of annual precipitation series shown in Table 3. Several findings are obtained. First, no abrupt changes occur in the distribution (Generalized Extreme Value) of annual precipitation series at all stations while significant abrupt changes appear in the mean (variance) value of annual precipitation series at 117 (49)

Table 3
Results of Multiple Methods at a Significance Level of 0.05 on the Abrupt Changes in the Distribution, Mean and Variance of Annual Precipitation Series at 159 Stations of Five Regions in Norway

| Region (stations) | Change point | Distribution | | | Mean | | Variance | |
|------------------------|--------------|------------------|--------------------|------------------|------------------------------------|-----------------------|----------------------|----------------------|
| | | Anderson Darling | Kolmogorov-Smirnov | Cramer-von Mises | Pettitt test | Mann-Whitney | Lombard Mood | Mood |
| East (49) ^a | Single | | | | 1980 (32) ^b 1982 (8) | 1980 (32) 1982 (8) | 1980 (9) 1982 (5) | 1980 (9) 1982 (5) |
| | Multiple | | | | | | | |
| | None | 49 ^c | 49 | 49 | 9 | 9 | 35 | 35 |
| South (11) | Single | | | | 1979 (10) | 1979 (10) | 1979 (5) | 1979 (5) |
| | Multiple | | | | | | | |
| | None | 11 | 11 | 11 | 1 | 1 | 6 | 6 |
| West (24) | Single | | | | 1979 (13) 1981 (5) | 1979 (13) 1981 (5) | 1979 (5) 1981 (2) | 1979 (5) 1981 (2) |
| | Multiple | | | | | | | |
| | None | 24 | 24 | 24 | 6 | 6 | 17 | 17 |
| Middle (22) | Single | | | | 1981 (11) 1984 (6) | 1981 (11) 1984 (6) | 1981 (6) 1984 (2) | 1981 (6) 1984 (2) |
| | Multiple | | | | | | | |
| | None | 22 | 22 | 22 | 5 | 5 | 14 | 14 |
| North (53) | Single | | | | 1981 (7) 1984 (25) | 1981 (7) 1984 (25) | 1981 (6) 1984 (9) | 1981 (6) 1984 (9) |
| | Multiple | | | | | 1981 and 1984 (7) | | |
| | None | 23 | 53 | 53 | 21 | 21 | 38 | 38 |

^aThe number in the square bracket is the total number of rainfall gauge stations in the region. ^bThe number in the bracket is the number of stations where annual precipitation series have change points. ^cThe number in the bracket is the number of stations where annual precipitation series have no change point.

out of 159 stations in five regions of Norway. Second, the annual precipitation series at most stations in four regions have two single change points apart from those of the southern region, while only 7 stations in the northern region have multiple (=2) change points. Third, there is a consensus among multiple comparison procedures in detection of changes in mean and variance parameters at a significance level of 0.05. Taking the eastern region as an example, both Pettitt and Mann-Whitney tests identify 1980 (1982) as a change point in the mean of annual precipitation series at 32 (8) stations while both Lombard Mood and Mood identify 1980 (1982) as a change point in the variance of annual precipitation series at 9 (5) stations.

For multiple change points (1981 and 1984) in annual precipitation series at the seven stations of the northern region, when the time interval (4 years) between two change points in the time series is less than 10 years, the change point (1984) closer to the current time is identified as the final one (Friedman et al., 2016). Therefore, the mean and variance of annual precipitation series have abrupt changes in 1979 in the southern region, 1979 and 1981 in the western region, 1980 and 1982 in the eastern region, 1981 and 1984 in the middle region, and 1984 in the northern region. Five time series plots corresponding to the five specified rainfall stations of five regions in Norway are used to further reveal abrupt changes in the mean or variance of annual precipitation series (Figure 3).

Second, detected change points were used to divide the entire time series into subsets, in which each subset and the entire time series would be tested for the occurrence of monotonic trends. Table 4 summarizes the results of the Mann-Kendall Test at a significance level of 0.05 on the trend changes in the annual precipitation series at 159 stations of five regions in Norway. It is easy to find that none of the first segment in the annual precipitation series at 117 stations has a monotonic trend while both the second segment and the entire time series with a change point have significant increasing trends. Besides, the annual precipitation series at the other 42 stations have neither change points nor monotonic trends at a significance level of 0.05. The results demonstrate that abrupt change

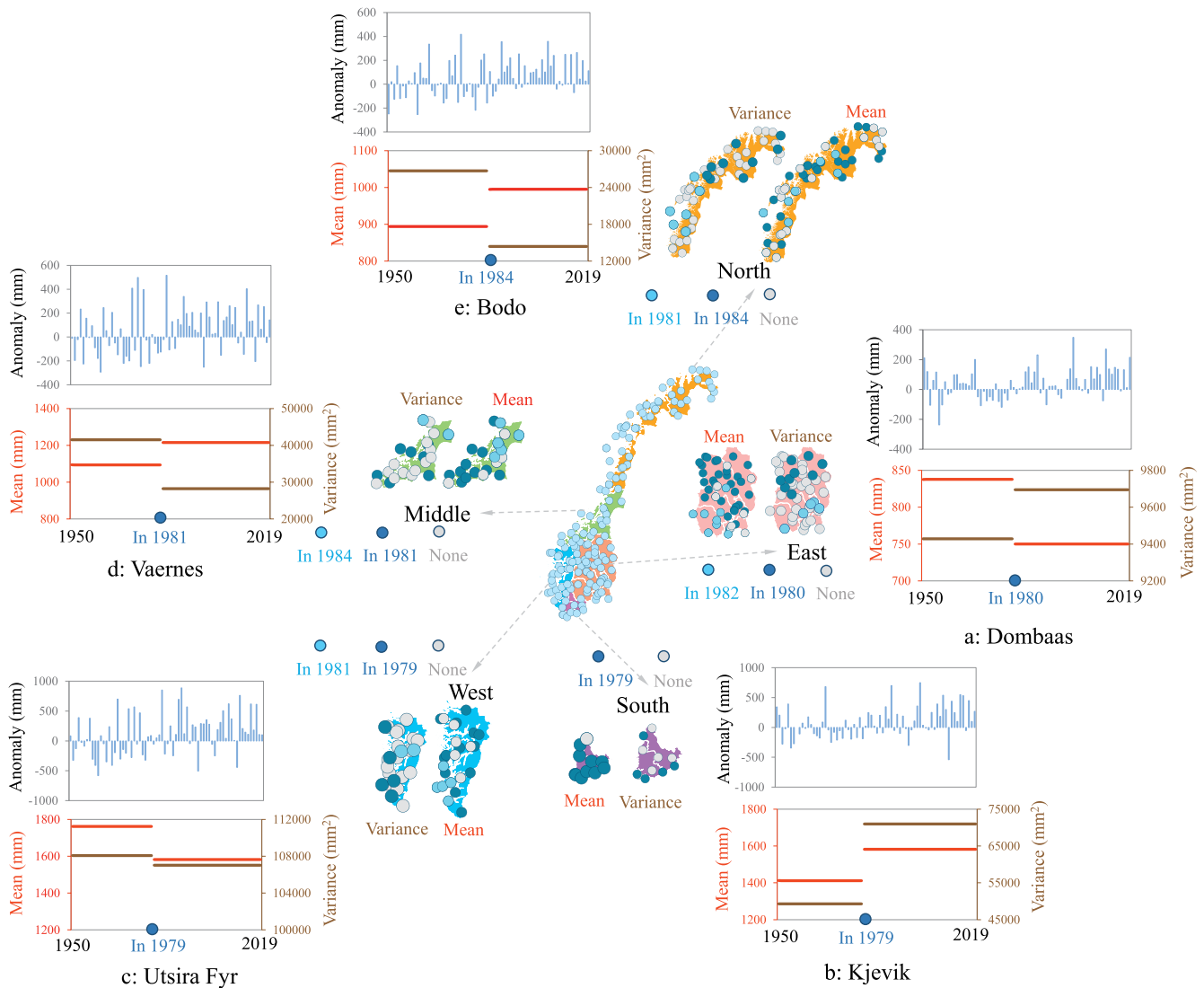


Figure 3. Abrupt changes in the mean or variance of annual precipitation series corresponding to the five specified rainfall stations of five regions in Norway (a. Dombaas in the east; b. Kjevnik in the south; c. Utsira Fyr in the west; d. Vaernes in the middle; and e. Bodo in the north) at a significance level of 0.05.

detection should be executed prior to trend analysis for effectively ascertaining the nonstationary characteristics in every segment and the entire time series.

Figure 4 reveals the observed trends in mean and variance of annual precipitation series corresponding to the 159 rainfall stations in five regions of Norway during the second segment (in the wake of the change point) in comparison to those of the first segment (prior to the change point). Two important findings are gained. First, the changes in the mean of annual precipitation series in eastern, southern and western regions are distinguishably larger than those in middle and northern regions. Second, the mean and variance of annual precipitation series increase by 32% and 16% at most, respectively.

Previous analyses concentrated mainly on detecting the global trends of the entire precipitation series, where no increasing trends were identified in the segments of precipitation series at a Norwegian scale (Dyrrdal et al., 2016; Ingebrigtsen et al., 2014, 2015). At local and regional scales (for instance, Porsanger fjord and southern Norway) and in several periods (for instance, summer and winter), increasing trends of the entire precipitation series were identified (Blanchet et al., 2015; Cieszyńska & Stramska, 2018; Dyrrdal et al., 2016). Our findings provide clear evidence that the mean (variance) values of annual precipitation series at 122 (49) stations have significant

Table 4
Results of the Mann-Kendall Test at a Significance Level of 0.05 on the Trend Changes in the Annual Precipitation Series at the 159 Stations of Five Regions in Norway

| Region (stations) | Time series | Trend analysis | | |
|------------------------|--|-----------------|------------|-----------------|
| | | Increasing | Decreasing | Neither |
| East (49) ^a | First segment (Prior to 1980 or 1982) ^b | | | 40 ^c |
| | Second segment | 40 ^d | | |
| | Entire series | 40 | | 9 |
| South (11) | First segment (Prior to 1979) | | | 10 |
| | Second segment | 10 | | |
| | Entire series | 10 | | 1 |
| West (24) | First segment (Prior to 1979 or 1981) | | | 18 |
| | Second segment | 18 | | |
| | Entire series | 18 | | 6 |
| Middle (22) | First segment (Prior to 1981 or 1984) | | | 17 |
| | Second segment | 17 | | |
| | Entire series | 17 | | 5 |
| North (53) | First segment (Prior to 1984) | | | 32 |
| | Second segment | 32 | | |
| | Entire series | 32 | | 21 |

^aThe number in the square bracket is the total number of rainfall gauge stations in a region. ^bTake 1950–2019 time series and change point in 1980 as an example, the first segment, the second segment and the entire series are 1950–1980, 1981–2019, and 1950–2019, respectively. ^cThe number of stations where annual precipitation series have no change in trends. ^dThe number of stations where annual precipitation series have increasing trends.

increasing trends across Norway over the past 70 years, corresponding to the second segment of annual precipitation series.

Third, the Wavelet Analysis was used to detect periodicity values of annual precipitation series. Table 5 presents the periodicity values detected by the Wavelet Analysis on the annual precipitation series at the 159 stations of five regions in Norway. There are strong temporal patterns of annual precipitation series at most stations in five regions of Norway, with two consistent temporal patterns at most stations and no temporal pattern at 32 stations during 1950–2019. For instance, a strong temporal pattern is found at scales of 40–50 years, while a less significant temporal pattern exhibited at scales of 20–30 years for annual precipitation series at stations of the eastern region. On the other hand, annual precipitation series from southern and western regions have large values of the first periodicity (45–55 years) while those from eastern and southern regions have small values of the second periodicity (20–30 years).

To be more specific, Figure 5 reveals the periodicity scale and wavelet variance of wavelet analysis on annual precipitation series (1950–2019) with respect to the five specified rainfall stations of five regions (a. Dombaas in the east; b. Kjevik in the south; c. Utsira Fyr in the west; d. Vaernes in the middle; and e. Bodo in the north) in Norway. It can be observed from the subfigures that the Wavelet Analysis can effectively capture the nonstationary temporal patterns corresponding to specific time localizations for annual precipitation series at five stations. According to the changes in real wavelet coefficients (left subfigures), both the first and the second periodicities with respect to annual precipitation series at five stations have the continuous hydrological alteration between wet and dry years. In addition, from the perspective of the wavelet variance (right subfigures), the first and the second periodicities correspond to the first and the second peaks of wavelet variance, respectively. Therefore, it is easy to find that the annual precipitation series at five stations have the first periodicities (a: 43 years; b: 48 years; c: 48 years; d: 44 years; and e: 45 years) and the second periodicities (a: 24 years; b: 27 years; c: 31 years; d: 30 years; and e: 32 years).

In brief, the first periodicity (40–50 years or 45–55 years) is the dominant periodic component that can be used to best describe the nonstationary annual precipitation series at the stations of five regions in Norway.

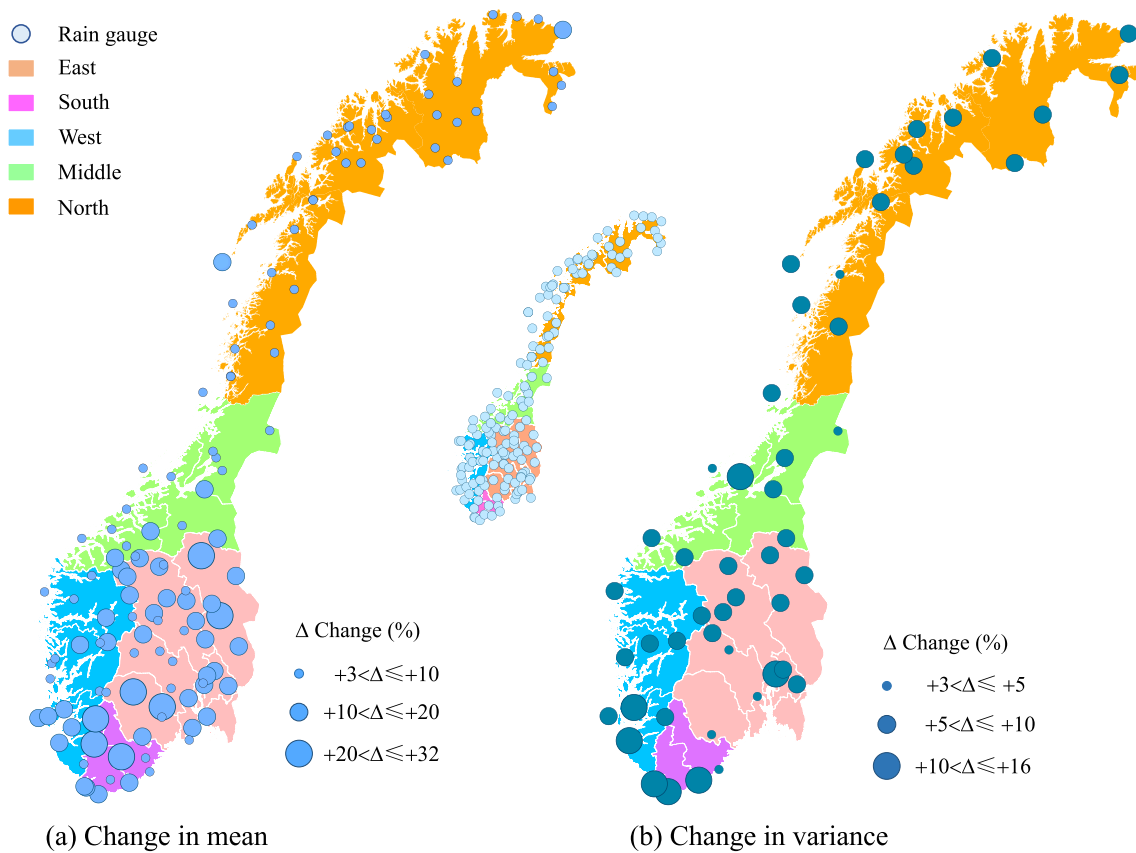


Figure 4. Observed trends in mean and variance of annual precipitation series corresponding to the 159 rainfall stations in five regions of Norway during the second segment (in the wake of the change point) in comparison to those of the first segment (prior to the change point).

4.2. Attribution Analysis of Nonstationary Annual Precipitation Series

Since the MIC can describe not only linear correlation but also nonlinear correlation, its values between annual precipitation and teleconnection series were calculated to explain the variability of annual precipitation series (Table 6). Considering teleconnection indices with a spatial resolution of $0.5^\circ \times 0.5^\circ$, the teleconnection value of a grid box that is the closest to a rainfall station was adopted to calculate the MIC value.

It is interesting to find that the annual precipitation series of all stations in five regions have higher correlation with SCAND and AMO series but have lower correlation with EAWR, NAO and MJO series in terms of MIC values. This kind of correlation must depend more on annual (SCAND) and interannual-to-decadal (AMO) oscillations than on seasonal oscillation. Therefore, it is logical to that the same correlation can be explained by oceanic teleconnection indices, instead of winter circulation teleconnection indices. Another interesting outcome is that high MIC values for annual precipitation series with SCAND and AMO series are obtained for eastern, southern and western regions, while low values appear in middle and northern regions.

The main types of precipitation include rain, sleet, snow, ice pellets, and hail. The mean annual precipitation values in eastern, southern and western regions are prominently larger than those of middle and northern regions. In contrast, the mean annual snowfall values in eastern, southern and western regions are distinguishably smaller than those of middle and northern regions. The liquid form of precipitation is more sensible to oceanic indices than to winter circulation indices (Blanchet et al., 2015). Therefore, higher

Table 5
Periodicity Values Detected by the Wavelet Analysis on the Annual Precipitation Series at 159 Stations of Five Regions in Norway

| Region (stations) | Periodicity | | |
|------------------------|-------------------------------|------------------|----------------|
| | First | Second | Neither |
| East (49) ^a | 40–50 years (34) ^b | 20–30 years (41) | 8 ^c |
| South (11) | 45–55 years (8) | 20–30 years (11) | 0 |
| West (24) | 45–55 years (16) | 25–35 years (19) | 5 |
| Middle (22) | 40–50 years (14) | 25–35 years (17) | 5 |
| North (53) | 40–50 years (39) | 25–35 years (39) | 14 |

^aThe number in the square bracket is the total number of rainfall gauge stations in a region. ^bThe number of stations where annual precipitation series have periodicities. ^cThe number of stations where annual precipitation series have no periodicity.

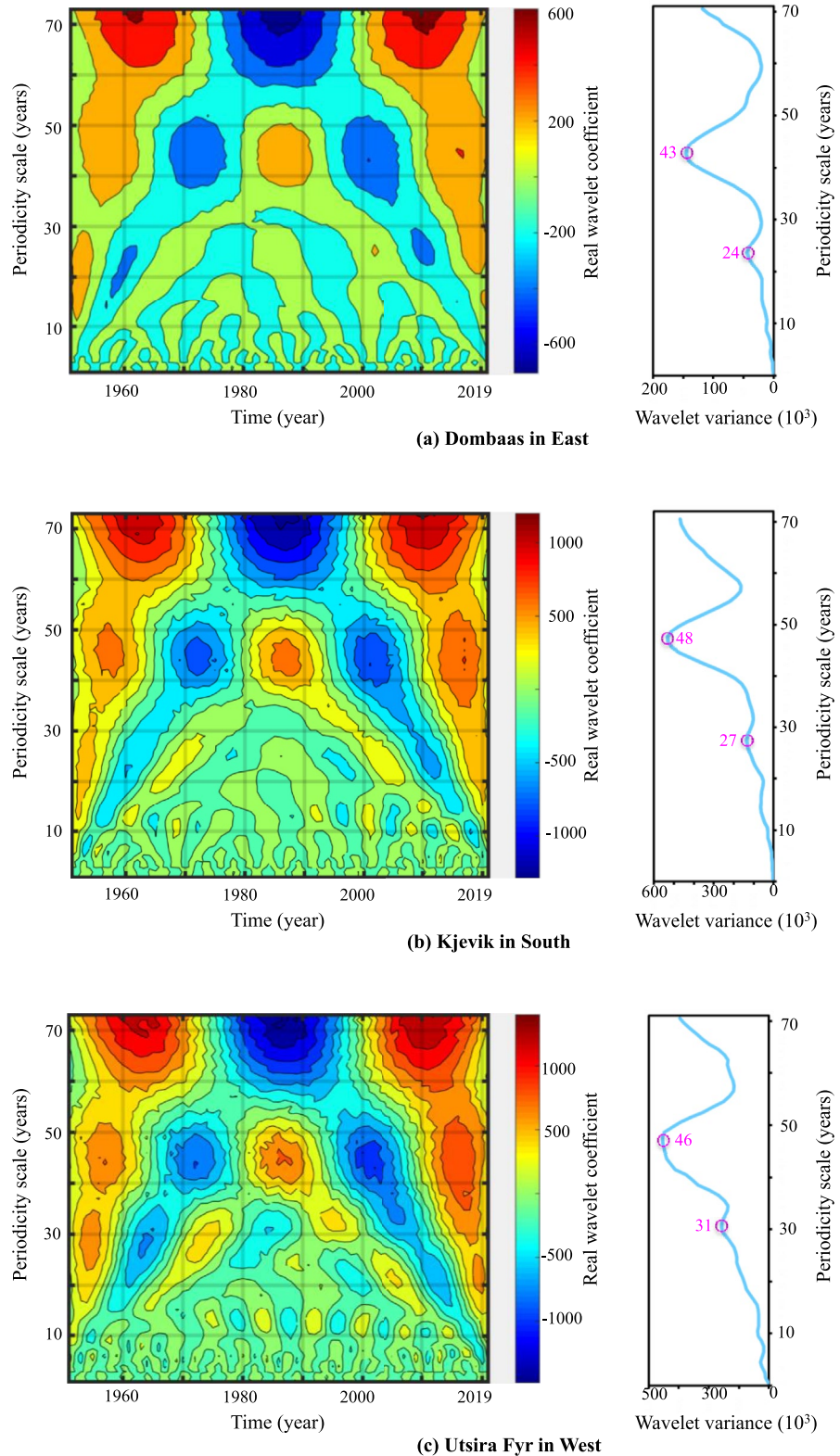


Figure 5. Periodicity scale and wavelet variance in wavelet analysis of annual precipitation series (1950–2019) corresponding to the five specified rainfall stations (a. Dombaas in the east; b. Kjevik in the south; c. Utsira Fyr in the west; d. Vaernes in the middle; and e. Bodo in the north) of five regions in Norway.

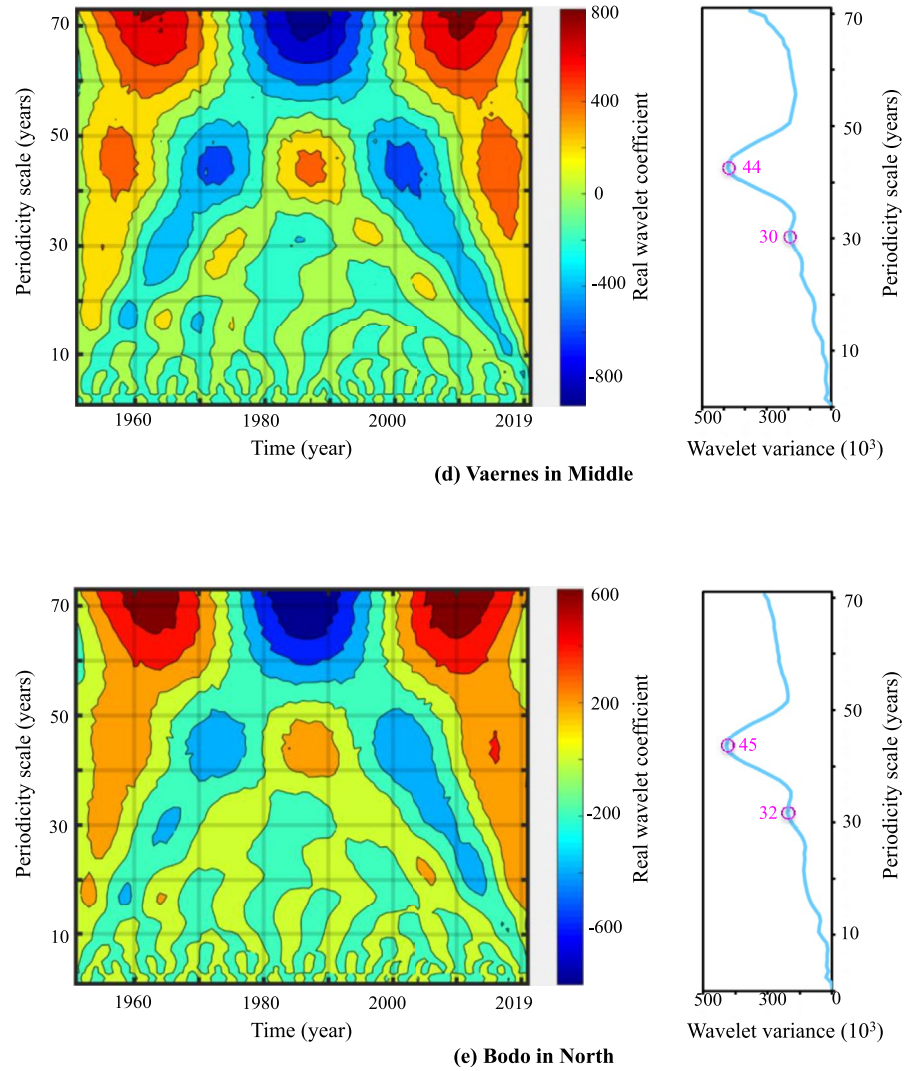


Figure 5. (Continued)

Table 6
Maximal Information Coefficient (MIC) Values Between Annual Precipitation and Teleconnection Series at Rainfall Stations in Five Regions of Norway

| Region (stations) | Annual oscillations | | | Interannual-to-decadal oscillations | |
|---------------------------|---------------------|------------------|------------------|-------------------------------------|------------------|
| | SCAND | NAO | EAWR | AMO | MJO |
| | Mean (Min–Max) | Mean (Min–Max) | Mean (Min–Max) | Mean (Min–Max) | Mean (Min–Max) |
| East (40/49) ^a | 0.72 (0.64–0.77) | 0.34 (0.28–0.38) | 0.29 (0.24–0.33) | 0.78 (0.67–0.84) | 0.26 (0.19–0.34) |
| South (10/11) | 0.76 (0.66–0.81) | 0.37 (0.25–0.42) | 0.34 (0.29–0.38) | 0.81 (0.71–0.87) | 0.31 (0.21–0.36) |
| West (18/24) | 0.69 (0.60–0.74) | 0.25 (0.18–0.29) | 0.31 (0.26–0.35) | 0.74 (0.62–0.79) | 0.22 (0.15–0.29) |
| Middle (17/22) | 0.62 (0.55–0.69) | 0.31 (0.23–0.35) | 0.22 (0.18–0.27) | 0.68 (0.59–0.73) | 0.27 (0.20–0.31) |
| North (32/53) | 0.58 (0.51–0.66) | 0.26 (0.21–0.30) | 0.28 (0.21–0.34) | 0.64 (0.56–0.75) | 0.19 (0.16–0.27) |

^aValues in the square bracket is the number of rainfall gauge stations in a region, where annual precipitation series have abrupt and trend changes at the same time versus the total number of stations in the region.

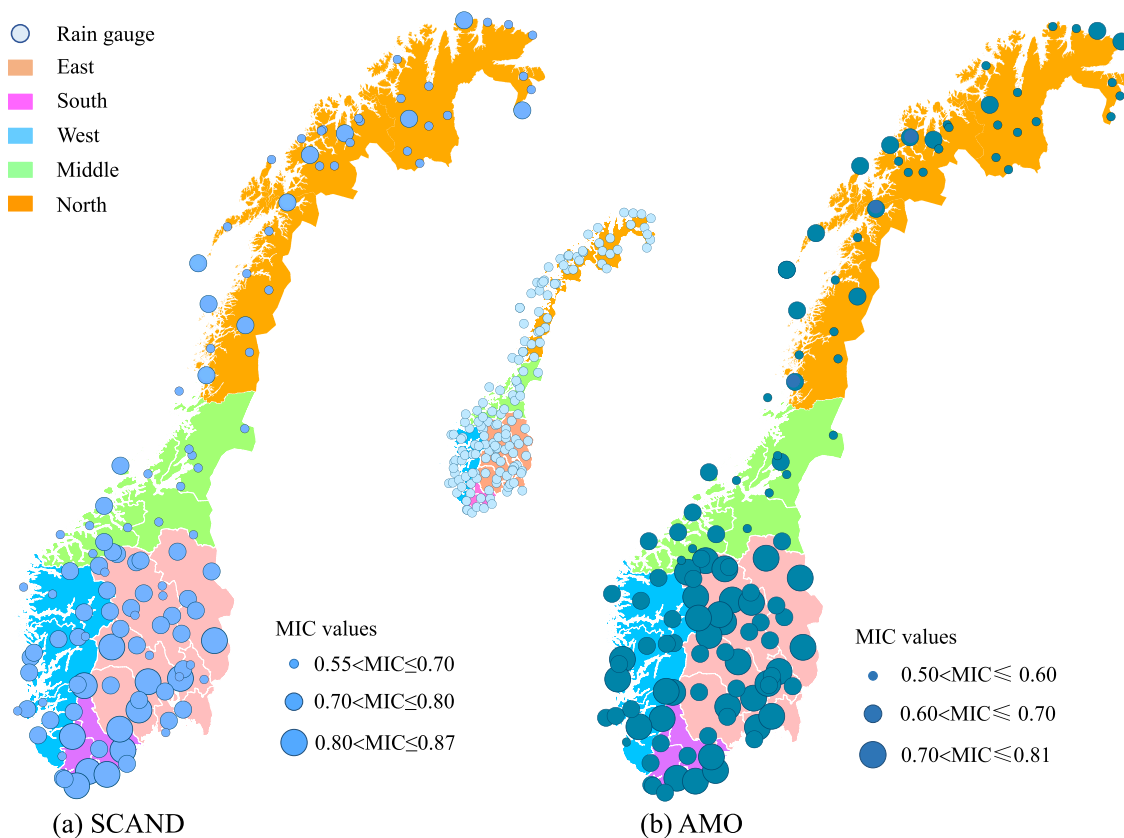


Figure 6. Spatial distribution of maximal information coefficient (MIC) values between annual precipitation series and the (a) Scandinavian pattern (SCAND) and (b) Atlantic Multidecadal Oscillation (AMO) series.

correlation of annual precipitation series with the SCAND and AMO series (oceanic indices) occurs in eastern, southern and western regions (Figure 6). In other words, stronger phases of SCAND and AMO series give rise to more annual precipitation and significant variability in those regions. The results reveal that the variability of annual precipitation series is eminently associated with the northern hemisphere annual and interannual-to-decadal oscillations. Changes in rain-on-snow events typically contribute to the majority of flooding in middle and northern regions (Li et al., 2019), and the attribution to interconnection is also important (Pall et al., 2019).

In this study, the Python 3.8 software was used to visualize the kernel density estimation of the joint distribution between the annual precipitation series and the teleconnection indices. Figure 7 exhibits the kernel density estimation of the joint distribution between the annual precipitation series (1950–2019) and the SCAND and AMO series corresponding to the five specified rainfall stations (a. Dombaas in the east; b. Kjevik in the south; c. Utsira Fyr in the west; d. Vaernes in the middle; and e. Bodo in the north) of five regions in Norway. Three important findings are noted. First, the positive and negative phases of SCAND and AMO series are closely associated with annual precipitation series over five regions of Norway. Second, the upward hook structure (left subfigures) appears in the correlation between the annual precipitation and the SCAND series. In contrast, the downward hook structure (right subfigures) occurs in the correlation between the annual precipitation and the AMO series. Third, the northern hemisphere annual (SCAND) and interannual-to-decadal (AMO) oscillations can reasonably explain the causes of nonstationary annual precipitation series during 1950 and 2019 in terms of the MIC values (0.60–0.82). Such hook structures are probably due to the variation in sea level pressure, where the subtropical Azores High (subpolar Icelandic Low) tends to move toward (away from) Europe (Börgel et al., 2020; Casanueva et al., 2014).

Table 7 summarizes the calculated MIC values between real wavelet coefficients of each periodicity and SCAND and AMO series at the rainfall stations in five regions of Norway. The wavelet coefficients of the first periodicity have higher correlation coefficient values for all stations of five regions. The wavelet coefficients of the second

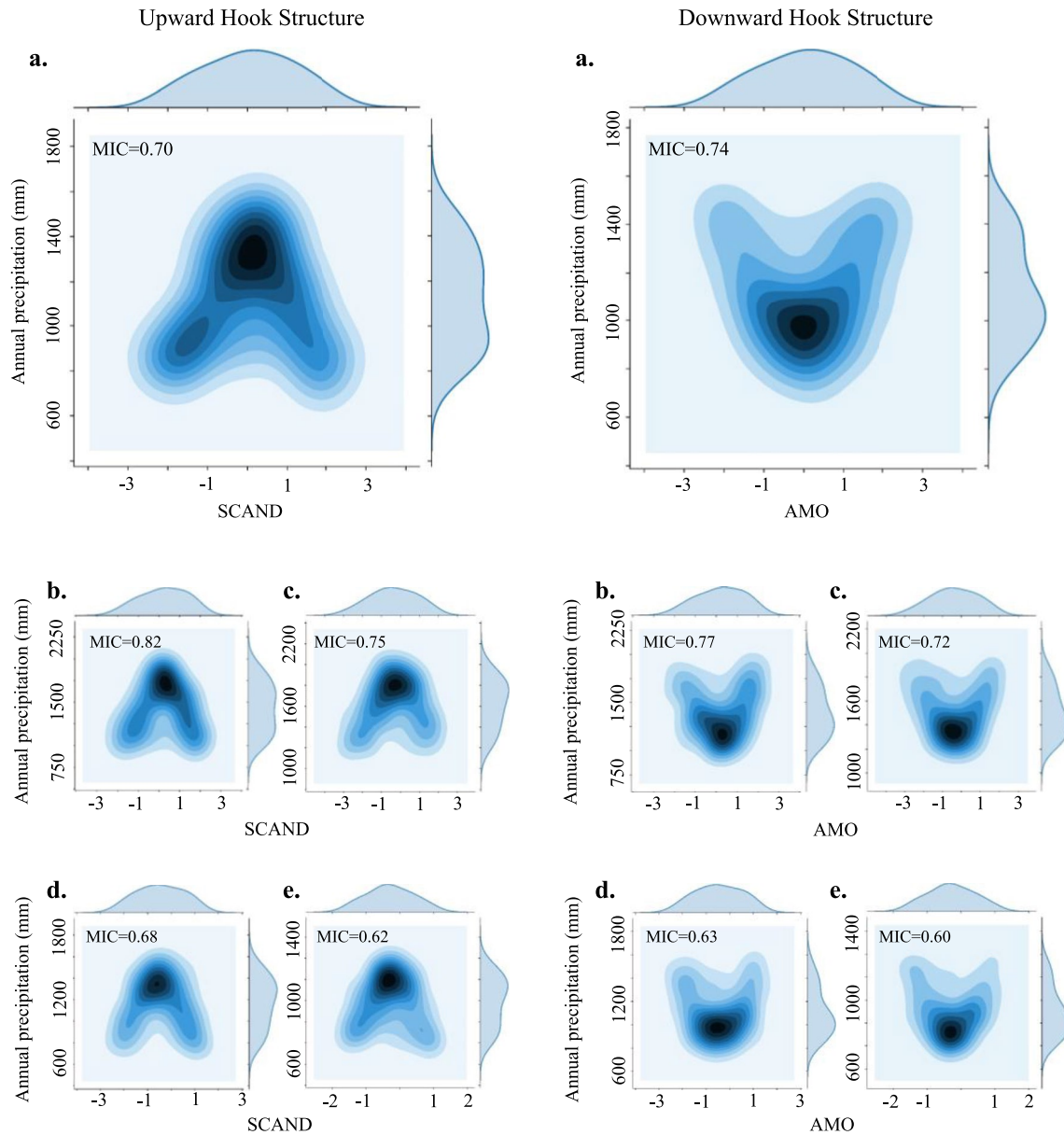


Figure 7. Kernel density estimation of the joint distribution between the annual precipitation series (1950–2019) and the Scandinavian pattern (SCAND) and Atlantic Multidecadal Oscillation (AMO) series corresponding to the five specified rainfall stations (a. Dombaas in the east; b. Kjevik in the south; c. Utsira Fyr in the west; d. Vaernes in the middle; and e. Bodo in the north) of five regions in Norway.

periodicity display lower correlation coefficient values for all stations of five regions. The correlation results again demonstrate that the first periodicity (40–50 years or 45–55 years) is the dominant periodic component. Such periodic component can be used to best describe the annual precipitation series of five regions in Norway. Furthermore, the periodic characteristics of the annual precipitation series at the stations of five regions in Norway can be attributed to the northern hemisphere annual (SCAND) and interannual-to-decadal (AMO) oscillations in terms of the MIC values. This study concentrates on analyzing annual scale factors instead of seasonal scale factors. At an annual scale SCAND and AMO are considered to be the driving factors. At a seasonal scale El Niño-Southern Oscillation (ENSO) and NAO are considered to have influences on summer and winter precipitation, respectively (Craig & Allan, 2021; Seager et al., 2020; Uvo, 2003).

In general, the SCAND and AMO series that are two of the most prominent oscillations of climatic variability in North Atlantic areas significantly influence Norwegian precipitation. Whereas previous studies (e.g., Asong

Table 7

Maximal Information Coefficient (MIC) Values Between Real Wavelet Coefficients of Each Periodicity and the Scandinavian Pattern (SCAND) and Atlantic Multidecadal Oscillation (AMO) Series at Rainfall Stations in Five Regions of Norway

| Region | MIC value between wavelet coefficients and SCAND series | |
|--------|---|----------------------------|
| | For the first periodicity | For the second periodicity |
| | Mean (Min–Max) | Mean (Min–Max) |
| East | 0.71 (0.50–0.81) | 0.39 (0.21–0.48) |
| South | 0.76 (0.58–0.87) | 0.32 (0.24–0.41) |
| West | 0.73 (0.52–0.84) | 0.35 (0.20–0.43) |
| Middle | 0.64 (0.53–0.77) | 0.41 (0.32–0.49) |
| North | 0.68 (0.55–0.79) | 0.37 (0.29–0.46) |
| Region | MIC value between wavelet coefficients and AMO series | |
| | For the first periodicity | For the second periodicity |
| | Mean (Min–Max) | Mean (Min–Max) |
| East | 0.66 (0.46–0.74) | 0.33 (0.23–0.41) |
| South | 0.73 (0.52–0.82) | 0.31 (0.26–0.39) |
| West | 0.71 (0.48–0.75) | 0.29 (0.21–0.37) |
| Middle | 0.61 (0.44–0.72) | 0.38 (0.29–0.45) |
| North | 0.65 (0.49–0.77) | 0.34 (0.27–0.43) |

et al., 2018; Blöschl et al., 2020; Nalley et al., 2019) concentrated on attributing Norwegian precipitation trend change, this study proffers a comprehensive perspective and explores annual and interannual-to-decadal teleconnections for explaining the causes of abrupt changes, trends and periodicities of annual precipitation series. The SCAND and AMO series can affect regional climatic patterns in the Northern Hemisphere and account for most of the precipitation variability over the Northern European and North Atlantic areas. The SCAND and AMO series also explain most of the precipitation variability for the whole Norway mainland over annual and decadal time scales.

In summary, our study indicates that the proposed approach can help detect the abrupt change, trend and periodicity of annual precipitation series meanwhile suitably explain the causes of the nonstationary characteristics associated with northern hemisphere annual and interannual-to-decadal oscillations.

5. Conclusions

Understanding the nonstationarity of precipitation time series and their correlation with atmospheric processes can help improve the resilience of stormwater infrastructure, community, and living conditions in response to climate change. In this study, multiple comparison procedures, that is, the Mann-Kendall test and the Wavelet Analysis, were adopted to detect the variability characteristics (abrupt change, trend and periodicity) of the annual precipitation series at 159 rainfall stations of five regions in Norway. The MIC-based correlation analysis was employed to explain the causes of the nonstationarity in long term (1950–2019) annual precipitation series from the standpoint of atmospheric teleconnection. The findings of this study are summarized as follows.

At a significance level of 0.05, no abrupt changes are observed in the distribution of annual precipitation series at all stations. Significant abrupt changes occur in the mean (variance) value of annual precipitation series at 117 (49) out of 159 stations of five regions in Norway. The change points in the annual precipitation series vary from 1979 to 1984.

At a significance level of 0.05, the mean (variance) values of annual precipitation series at 117 (49) out of 159 stations show noticeably increasing trends. The changes in the mean of the annual precipitation series at eastern, southern and western regions are distinguishably larger than those in middle and northern regions. The changes in the variance of the annual precipitation series in five regions are evenly distributed. The changes in the mean and

variance of annual precipitation series in the wake of change points fall within the intervals of [+3%, +32%] and [+3%, +16%], respectively, in comparison to those of annual precipitation series prior to change points.

Two consistent temporal patterns of annual precipitation series are noticed for most rainfall stations in five regions of Norway. The first periodicity varies between 40 and 50 years (or 45–55 years) while the second periodicity varies between 20 and 30 years (or 25–35 years). The first periodicity (40–50 years or 45–55 years) is the dominant periodic component and can be employed to best characterize the nonstationary annual precipitation series at the stations of five regions in Norway.

Two consistent correlation structures are identified. The correlation between the annual precipitation series and the SCAND series forms an upward hook structure because the subtropical Azores High moves toward Europe. The correlation between the annual precipitation series and the AMO series tends to have a downward hook structure because the subpolar Icelandic Low moves away from Europe. The northern hemisphere annual (SCAND) and interannual-to-decadal (AMO) oscillations can reasonably explain the causes of nonstationary annual precipitation series in terms of the MIC values.

Detection and attribution of nonstationary precipitation series could assist in understanding the variability of precipitation series and their associations with teleconnection indices. It also paves the way for new possibilities regarding nonstationary hydrological frequency analysis. This study utilizes the bivariate correlation analysis to explain the impacts of atmospheric processes on precipitation nonstationarity. The MIC aims to detect associations in large data sets. The computation accuracy of the MIC is limited to the sample size. The larger the sample size, the higher the computation accuracy of the MIC. More extensive research to warrant the effect of sample size on the computation accuracy of the MIC will be explored in the future.

Appendix A: Prewhitening-Based Mann-Kendall Test

An autocorrelation would not guarantee to identify a time series when it has a trend. The autocorrelation coefficient with lag- k is described as follows.

$$r_k = \frac{\sum_{k=1}^{m-k} (z_t - \bar{z}_t) \cdot (z_{t+k} - \bar{z}_{t+k})}{\sum_{t=1}^{m-k} (z_t - \bar{z}_t)^2 \cdot \sum_{m-}^{t=1} (z_{t+k} - \bar{z}_{t+k})^2} \quad (\text{A1})$$

where r_k is the autocorrelation coefficient with lag- k . m is the number of data points within a time series. z_t and z_{t+k} are the sample values of the first $m-k$ terms and the last $m-k$ terms in a time series, respectively. \bar{z}_t and \bar{z}_{t+k} are the mean values of the first $m-k$ terms and the last $m-k$ terms in a time series, respectively. Additionally, the Student's t statistical test is adopted to test the hypothesis of serial dependence for the autocorrelation coefficient r_k as the null hypothesis $H_0: r_k = 0$, and the alternative hypothesis $H_1: r_k \neq 0$. The statistic of the test is described below.

$$td = |r_k| \cdot \sqrt{\frac{m-2}{1-r_k^2}} \quad (\text{A2})$$

where td is the statistic of the test, which has a Student's t -distribution with $m-2$ degrees of freedom. When $|td| > t_{\frac{\alpha}{2}}$ occurs, the null hypothesis H_0 will be rejected at the significant level α . That is to say, the significant autocorrelation appears in a time series.

For annual precipitation time series P_t , the lag-1 autocorrelation coefficient (r_1) is commonly used to remove serial autocorrelation (Yue et al., 2003).

$$P'_t = X_t - r_1 \cdot P_{t-1} \quad (\text{A3})$$

where r_1 is the lag-1 autocorrelation coefficient. P'_t is the corrected precipitation time series by using the lag-1 autocorrelation coefficient in the t th time.

After eliminating serial correlation, the Mann-Kendall test is adopted to identify statistically significant trends for a time series. In the Mann-Kendall test, the null hypothesis H_0 is that there is no trend in a time series while the alternative hypothesis H_1 is that there is a (decreasing or increasing) trend over time. The computations of Mann-Kendall statistic S , variance of S , and standardized normal statistic Z are described as follows.

$$S = \sum_{i=1}^{m-1} \sum_{j=i+1}^m \text{sig}(p_j - p_i) \quad (\text{A4a})$$

$$\text{sig}(p_j - p_i) = \begin{cases} +1, & \text{if}(p_j - p_i) > 0 \\ 0, & \text{if}(p_j - p_i) = 0 \\ -1, & \text{if}(p_j - p_i) < 0 \end{cases} \quad (\text{A4b})$$

$$\text{Var}(S) = \frac{1}{18} [m \cdot (m - 1) \cdot (2m + 5) - \sum_{i=1}^q t_i \cdot (t_i - 1) \cdot (2t_i + 5)] \quad (\text{A5})$$

$$Z = \begin{cases} \frac{S - 1}{\sqrt{\text{Var}(S)}}, & \text{if } S > 0 \\ 0, & \text{if } S = 0 \\ \frac{S + 1}{\sqrt{\text{Var}(S)}}, & \text{if } S < 0 \end{cases} \quad (\text{A6})$$

where $\text{sig}(\cdot)$ is the sign function. p_i and p_j are the observations of time series in chronological order. $\text{Var}(S)$ is the variance of statistic S . q is the total number of tie groups in a time series. t_i is the number of data points contained in the i th tie group. Z is the standardized normal statistic. A positive value of statistic Z suggests an increasing trend in a time series while a negative one suggests a decreasing trend. When $|Z| > Z_{1-\alpha/2}$, where α is the significant level, the trend is statistically significant (e.g., $\alpha = 0.05$, and $Z_{1-\alpha/2} = 1.96$).

Data Availability Statement

Precipitation data extracted from the Global Summary of the Day (GSOD) datasets are accessible on the website of the National Climate Data Center (<https://catalog.data.gov/dataset/global-surface-summary-of-the-day-gsod>), the North Atlantic Oscillation (NAO), the East Atlantic/Western Russia pattern (EAWR) and the Atlantic Multidecadal Oscillation (AMO) are accessible on the website of the National Oceanic and Atmospheric Administration (<https://psl.noaa.gov/data/climateindices/list/>), the Scandinavian pattern (SCAND) is accessible on the website (<https://www.cpc.ncep.noaa.gov/data/teledoc/telecontents.shtml>), and the Madden-Julian Oscillation (MJO) is accessible on the website (https://www.cpc.ncep.noaa.gov/products/precip/CWlink/mjo_iso.html).

References

- Ahmad, I., Tang, D., Wang, T., Wang, M., & Wagan, B. (2015). Precipitation trends over time using Mann-Kendall and Spearman's rho tests in the Swat River Basin, Pakistan. *Advances in Meteorology*, *15*, 1–15. <https://doi.org/10.1155/2015/431860>
- Asong, Z. E., Wheeler, H. S., Bonsal, B., Razavi, S., & Kurkute, S. (2018). Historical drought patterns over Canada and their teleconnections with large-scale climate signals. *Hydrology and Earth System Sciences*, *22*, 3105–3124. <https://doi.org/10.5194/hess-22-3105-2018>
- Baidu, M., Amekudzi, L. K., Aryee, J. N. A., & Annor, T. (2017). Assessment of long-term spatio-temporal rainfall variability over Ghana using wavelet analysis. *Climate*, *5*(2), 30–36. <https://doi.org/10.3390/cli5020030>
- Bayazit, M., & Önöz, B. (2007). To prewhiten or not to prewhiten in trend analysis? *Hydrological Sciences Journal*, *52*(4), 611–624. <https://doi.org/10.1623/HYSJ.52.4.611>
- Blanchet, J., Touati, J., Lawrence, D., Garavaglia, F., & Paquet, E. (2015). Evaluation of a compound distribution based on weather pattern subsampling for extreme rainfall in Norway. *Natural Hazards and Earth System Sciences*, *15*, 2653–2667. <https://doi.org/10.5194/nhess-15-2653-2015>
- Blöschl, G., Kiss, A., Viglione, A., Barriendos, M., Böhm, O., Brázdil, R., et al. (2020). Current European flood-rich period exceptional compared with past 500 years. *Nature*, *583*(7817), 560–566. <https://doi.org/10.1038/S41586-020-2478-3>
- Börgel, F., Frauen, C., Neumann, T., & Meier, H. E. M. (2020). The Atlantic multidecadal oscillation controls the impact of the North Atlantic oscillation on North European climate. *Environmental Research Letters*, *15*(10), 104025. <https://doi.org/10.1088/1748-9326/ABA925>
- Cannon, A. J. (2010). A flexible nonlinear modelling framework for nonstationary generalized extreme value analysis in hydroclimatology. *Hydrological Processes*, *24*(6), 673–685. <https://doi.org/10.1002/hyp.7506>
- Casanueva, A., Rodríguez-Puebla, C., Frías, M. D., & González-Reviriego, N. (2014). Variability of extreme precipitation over Europe and its relationships with teleconnection patterns. *Hydrology and Earth System Sciences*, *18*, 709–725. <https://doi.org/10.5194/hess-18-709-2014>
- Chen, Y. N., Deng, H. J., Li, B. F., Li, Z., & Xu, C. C. (2014). Abrupt change of temperature and precipitation extremes in the arid region of Northwest China. *Quaternary International*, *336*, 35–43. <https://doi.org/10.1016/j.quaint.2013.12.057>
- Cieszyńska, A., & Stramska, M. (2018). Climate-related trends and meteorological conditions in the Porsanger fjord, Norway. *Oceanologia*, *60*(3), 344–366. <https://doi.org/10.1016/J.OCEANO.2018.01.003>

Acknowledgments

This work was supported by the National Key Research and Development Program of China (2021YFC3200303), the National Natural Science Foundation of China (No. 51525902, 51538173) and the Research Council of Norway (FRINATEK Project 274310, KLIMAFORSK Project 302457). The authors would like to thank the Editors and anonymous Reviewers for their constructive comments that are greatly contributive to enriching the manuscript. The computation of nonstationarity detection was completed on the R software platform (<https://cran.r-project.org/>). The computation of period analysis was completed on MathWorks (<https://www.mathworks.com/products/wavelet.html>). The computation of attribution analysis was completed on minepy (<https://github.com/minepy/minepy/releases>).

- Craig, P. M., & Allan, R. P. (2021). The role of teleconnection patterns in the variability and trends of growing season indices across Europe. *International Journal of Climatology*. <https://doi.org/10.1002/joc.7290>
- Delworth, T. L., & Zeng, F. (2016). The impact of the North Atlantic oscillation on climate through its influence on the Atlantic meridional overturning circulation. *Journal of Climate*, 29(3), 941–962. <https://doi.org/10.1175/JCLI-D-15-0396.1>
- Dyrddal, A. V., Isaksen, K., Hygen, H. O., & Meyer, N. K. (2012). Changes in meteorological variables that can trigger natural hazards in Norway. *Climate Research*, 55(2), 153–165. <https://doi.org/10.3354/CR011125>
- Dyrddal, A. V., Lenkoski, A., Thorarinsdottir, T. L., & Stordal, F. (2015). Bayesian hierarchical modeling of extreme hourly precipitation in Norway. *Environmetrics*, 26(2), 89–106. <https://doi.org/10.1002/ENV.2301>
- Dyrddal, A. V., Skaugen, T., Stordal, F., & Førland, E. J. (2016). Estimating extreme areal precipitation in Norway from a gridded dataset. *Hydrological Sciences Journal*, 61(3), 483–494. <https://doi.org/10.1080/02626667.2014.947289>
- Dyrddal, A. V., Stordal, F., & Lussana, C. (2018). Evaluation of summer precipitation from EURO-CORDEX fine-scale RCM simulations over Norway. *International Journal of Climatology*, 38(4), 1661–1677. <https://doi.org/10.1002/JOC.5287>
- El-Borie, M. A., El-Taher, A. M., Thabet, A. A., & Bishara, A. A. (2020). The interconnection between the periodicities of solar wind parameters based on the interplanetary magnetic field polarity (1967–2018): A cross wavelet analysis. *Solar Physics*, 295(9), 1–20. <https://doi.org/10.1007/S11207-020-01692-2>
- Erdman, C., & Emerson, J. W. (2007). bcp: An R package for performing a Bayesian analysis of change point problems. *Journal of Statistical Software*, 23(1), 1–13. <https://doi.org/10.18637/JSS.V023.I03>
- Førland, E. J., & Kristoffersen, D. (1989). Estimation of extreme precipitation in Norway. *Hydrology Research*, 20, 257–276. <https://doi.org/10.2166/NH.1989.0020>
- Friedman, D., Schechter, J., Sant-Miller, A. M., Mueller, C., Villarini, G., White, K. D., & Baker, B. (2016). *US army corps of engineers nonstationarity detection tool user guide*. US Army Corps of Engineers.
- Guo, A., Chang, J., Wang, Y., Huang, Q., Guo, Z., & Li, Y. (2020). Development of a partial copula-based algorithm for disclosing variability of dependence structures between hydro-meteorological factors under consideration of covariate-effect. *Journal of Hydrology*, 583, 124570. <https://doi.org/10.1016/J.JHYDROL.2020.124570>
- Hegdahl, T. J., Engeland, K., Steinsland, I., & Tallaksen, L. M. (2019). Streamflow forecast sensitivity to air temperature forecast calibration for 139 Norwegian catchments. *Hydrology and Earth System Sciences*, 23(2), 723–739. <https://doi.org/10.5194/HESS-23-723-2019>
- Hua, T., Zorita, E., Wang, X., Wang, N., & Zhang, C. (2019). Precipitation variability in the north fringe of East Asian Summer Monsoon during the past millennium and its possible driving factors. *Climate Dynamics*, 53(5), 2587–2602. <https://doi.org/10.1007/S00382-019-04643-1>
- Ingebretsen, R., Lindgren, F., & Steinsland, I. (2014). Spatial models with explanatory variables in the dependence structure. *Spatial Statistics*, 8, 20–38. <https://doi.org/10.1016/J.SPASTA.2013.06.002>
- Ingebretsen, R., Lindgren, F., Steinsland, I., & Martino, S. (2015). Estimation of a non-stationary model for annual precipitation in southern Norway using replicates of the spatial field. *Spatial Statistics*, 14, 338–364. <https://doi.org/10.1016/J.SPASTA.2015.07.003>
- Irannezhad, M., Liu, J., & Chen, D. (2020). Influential climate teleconnections for spatiotemporal precipitation variability in the Lancang-Mekong River basin from 1952 to 2015. *Journal of Geophysical Research*, 125(21). <https://doi.org/10.1029/2020JD033331>
- James, N. A., & Matteson, D. S. (2015). ecp: An R package for nonparametric multiple change point analysis of multivariate data. *Journal of Statistical Software*, 62(1), 1–25. <https://doi.org/10.18637/JSS.V062.I07>
- Júnior, S. F. A. X., da Silva Jale, J., Stosic, T., dos Santos, C. A. C., & Singh, V. P. (2020). Precipitation trends analysis by Mann-Kendall test: A case study of Paraíba, Brazil. *Brazilian Journal of Meteorology*, 35(2), 187–196. <https://doi.org/10.1590/0102-7786351013>
- Kang, S., & Lin, H. (2007). Wavelet analysis of hydrological and water quality signals in an agricultural watershed. *Journal of Hydrology*, 338(1), 1–14. <https://doi.org/10.1016/J.JHYDROL.2007.01.047>
- Kendall, M. G. (1938). A new measure of rank correlation. *Biometrika*, 30(1–2), 81–89. <https://doi.org/10.1093/BIOMET/30.1-2.81>
- Kendall, M. G. (1975). *Rank correlation methods* (4th ed.). Charles Griffin.
- Kinney, J. B., & Atwal, G. S. (2014). Equitability, mutual information, and the maximal information coefficient. *Proceedings of the National Academy of Sciences of the United States of America*, 111(9), 3354–3359. <https://doi.org/10.1073/PNAS.1309933111>
- Lee, D. E., Ting, M., Vigaud, N., Kushnir, Y., & Barnston, A. G. (2018). Atlantic multidecadal variability as a modulator of precipitation variability in the southwest United States. *Journal of Climate*, 31(14), 5525–5542. <https://doi.org/10.1175/JCLI-D-17-0372.1>
- Lee, J. H., Ramirez, J. A., Kim, T. W., & Julien, P. Y. (2019). Variability, teleconnection, and predictability of Korean precipitation in relation to large scale climate indices. *Journal of Hydrology*, 568, 12–25. <https://doi.org/10.1016/J.JHYDROL.2018.08.034>
- Lee, T., & Ouarda, T. B. M. J. (2010). Long-term prediction of precipitation and hydrologic extremes with nonstationary oscillation processes. *Journal of Geophysical Research*, 115. <https://doi.org/10.1029/2009JD012801>
- Li, D., Lettenmaier, D. P., Margulis, S. A., & Andreadis, K. (2019). The role of rain-on-snow in flooding over the conterminous United States. *Water Resources Research*, 55(11), 8492–8513. <https://doi.org/10.1029/2019WR024950>
- Li, J. Z., Wang, Y. X., Li, S. F., & Hu, R. (2015). A nonstationary standardized precipitation index incorporating climate indices as covariates. *Journal of Geophysical Research*, 120(23). <https://doi.org/10.1002/2015JD023920>
- Li, X., Wang, X., & Babovic, V. (2018). Analysis of variability and trends of precipitation extremes in Singapore during 1980–2013. *International Journal of Climatology*, 38(1), 125–141. <https://doi.org/10.1002/JOC.5165>
- Liu, X., Feng, X., Ciais, P., & Fu, B. (2020). Widespread decline in terrestrial water storage and its link to teleconnections across Asia and eastern Europe. *Hydrology and Earth System Sciences*, 24, 3663–3676. <https://doi.org/10.5194/hess-24-3663-2020>
- Mahajan, S., Evans, K. J., Branstetter, M. L., & Tang, Q. (2018). Model resolution sensitivity of the simulation of North Atlantic Oscillation teleconnections to precipitation extremes. *Journal of Geophysical Research*, 123(20), 11392–11409. <https://doi.org/10.1029/2018JD028594>
- Mann, H. B. (1945). Nonparametric tests against trend. *Econometrica*, 13(3), 245. <https://doi.org/10.2307/1907187>
- Mayta, V. C., Ambrizzi, T., Espinoza, J. C., & Dias, P. L. S. (2019). The role of the Madden-Julian oscillation on the Amazon Basin intraseasonal rainfall variability. *International Journal of Climatology*, 39(1), 343–360. <https://doi.org/10.1002/JOC.5810>
- Montanari, A., & Koutsoyiannis, D. (2014). Modeling and mitigating natural hazards: Stationarity is immortal. *Water Resources Research*, 50, 9748–9756. <https://doi.org/10.1002/2014wr016092>
- Murgulet, D., Valeriu, M., Hay, R. R., Tissot, P., & Mestas-Núñez, A. M. (2017). Relationships between sea surface temperature anomalies in the Pacific and Atlantic Oceans and South Texas precipitation and streamflow variability. *Journal of Hydrology*, 550, 726–739. <https://doi.org/10.1016/J.JHYDROL.2017.05.041>
- Nalley, D., Adamowski, J., Biswas, A., Gharabaghi, B., & Hu, W. (2019). A multiscale and multivariate analysis of precipitation and streamflow variability in relation to ENSO, NAO and PDO. *Journal of Hydrology*, 574, 288–307. <https://doi.org/10.1016/J.JHYDROL.2019.04.024>
- Pall, P., Tallaksen, L. M., & Stordal, F. (2019). A climatology of rain-on-snow events for Norway. *Journal of Climate*, 32(20), 6995–7016. <https://doi.org/10.1175/JCLI-D-18-0529.1>

- Papalexiou, S. M., & Montanari, A. (2019). Global and regional increase of precipitation extremes under global warming. *Water Resources Research*, 55(6), 4901–4914. <https://doi.org/10.1029/2018WR024067>
- Pearson, K. (1895). Note on regression and inheritance in the case of two parents. *Proceedings of the Royal Society of London*, 58, 240–242. <https://doi.org/10.1098/rspl.1895.0041>
- Pei, F., Wu, C., Liu, X., Hu, Z., Xia, Y., Liu, L.-A., et al. (2018). Detection and attribution of extreme precipitation changes from 1961 to 2012 in the Yangtze River Delta in China. *Catena*, 169, 183–194. <https://doi.org/10.1016/J.CATENA.2018.05.038>
- Reshef, D. N., Reshef, Y. A., Finucane, H. K., Grossman, S. R., Mcvean, G., Turnbaugh, P. J., et al. (2011). Detecting novel associations in large data sets. *Science*, 334(6062), 1518–1524. <https://doi.org/10.1126/science.1205438>
- Ross, G. J. (2015). Parametric and nonparametric sequential change detection in R: The cpm package. *Journal of Statistical Software*, 66(1), 1–20. <https://doi.org/10.18637/JSS.V066.I03>
- Russo, S., Dosio, A., Sterl, A., Barbosa, P., & Vogt, J. (2013). Projection of occurrence of extreme dry-wet years and seasons in Europe with stationary and nonstationary Standardized Precipitation Indices. *Journal of Geophysical Research*, 118(14), 7628–7639. <https://doi.org/10.1002/JGRD.50571>
- Salas, J. D. (1993). Analysis and modeling of hydrologic time series. In *Handbook of hydrology*. McGraw-Hill.
- Sang, Y.-F., Singh, V. P., Gong, T., Xu, K., Sun, F., Liu, C., et al. (2016). Precipitation variability and response to changing climatic condition in the Yarlung Tsangpo River basin, China. *Journal of Geophysical Research*, 121(15), 8820–8831. <https://doi.org/10.1002/2016JD025370>
- Sarojini, B. B., Stott, P. A., & Black, E. (2016). Detection and attribution of human influence on regional precipitation. *Nature Climate Change*, 6(7), 669–675. <https://doi.org/10.1038/NCLIMATE2976>
- Seager, R., Liu, H., Kushnir, Y., Osborn, T. J., Simpson, I. R., Kelley, C. R., & Nakamura, J. (2020). Mechanisms of winter precipitation variability in the European-Mediterranean region associated with the North Atlantic oscillation. *Journal of Climate*, 33(16), 7179–7196. <https://doi.org/10.1175/JCLI-D-20-00111.1>
- Shannon, C. E. (1948). A mathematical theory of communication. *Bell System Technical Journal*, 27(3), 379–423. <https://doi.org/10.1002/J.1538-7305.1948.TB01338.X>
- Skogseth, R., Olivier, L. L. A., Nilsen, F., Falck, E., Fraser, N. J., Tverberg, V., et al. (2020). Variability and decadal trends in the Isfjorden (Svalbard) ocean climate and circulation: An indicator for climate change in the European Arctic. *Progress in Oceanography*, 187, 102394. <https://doi.org/10.1016/J.POCEAN.2020.102394>
- Song, M.-H., Li, K.-H., & Kim, S.-N. (2018). Evaluation of periodicities and fractal characteristics by wavelet analysis of well log data. *Computers & Geosciences*, 119, 29–38. <https://doi.org/10.1016/J.CAGEO.2018.05.002>
- Spearman, C. (1904). The proof and measurement of association between two things. *American Journal of Psychology*, 15(1), 72–101. <https://doi.org/10.2307/1412159>
- Sun, F., Roderick, M. L., & Farquhar, G. D. (2018). Rainfall statistics, stationarity, and climate change. *Proceedings of the National Academy of Sciences of the United States of America*, 115(10), 2305–2310. <https://doi.org/10.1073/PNAS.1705349115>
- Székely, G. J., Rizzo, M. L., & Bakirov, N. K. (2007). Measuring and testing independence by correlation of distances. *Annals of Statistics*, 35(6), 2769–2794. <https://doi.org/10.1214/009053607000000505>
- Tan, X., Gan, T. Y., & Shao, D. (2016). Wavelet analysis of precipitation extremes over Canadian ecoregions and teleconnections to large-scale climate anomalies. *Journal of Geophysical Research*, 121(24), 14486. <https://doi.org/10.1002/2016JD025533>
- Temmerud, J., & Weyhenmeyer, G. A. (2008). Abrupt changes in air temperature and precipitation: Do they matter for water chemistry? *Global Biogeochemical Cycles*, 22(2). <https://doi.org/10.1029/2007GB003023>
- Torres-Batló, J., & Martí-Cardona, B. (2020). Precipitation trends over the southern Andean Altiplano from 1981 to 2018. *Journal of Hydrology*, 590, 125485. <https://doi.org/10.1016/j.jhydrol.2020.125485>
- Uvo, C. B. (2003). Analysis and regionalization of northern European winter precipitation based on its relationship with the North Atlantic oscillation. *International Journal of Climatology*, 23(10), 1185–1194. <https://doi.org/10.1002/joc.930>
- Valdés-Pineda, R., Cañón, J., & Valdés, J. B. (2018). Multi-decadal 40- to 60-year cycles of precipitation variability in Chile (South America) and their relationship to the AMO and PDO signals. *Journal of Hydrology*, 556, 1153–1170. <https://doi.org/10.1016/J.JHYDROL.2017.01.031>
- Vicente-Serrano, S. M., & López-Moreno, J. I. (2008). Nonstationary influence of the North Atlantic oscillation on European precipitation. *Journal of Geophysical Research*, 113. <https://doi.org/10.1029/2008JD010382>
- Wathen, S. F. (2011). 1,800 Years of abrupt climate change, severe fire, and accelerated erosion, Sierra Nevada, California, USA. *Climatic Change*, 108, 333–356. <https://doi.org/10.1007/s10584-011-0046-4>
- Wu, Q., & Hu, Q. (2015). Atmospheric circulation processes contributing to a multidecadal variation in reconstructed and modeled Indian monsoon precipitation. *Journal of Geophysical Research*, 120(2), 532–551. <https://doi.org/10.1002/2014JD022499>
- Yan, L., Xiong, L., Ruan, G., Xu, C.-Y., Yan, P., & Liu, P. (2019). Reducing uncertainty of design floods of two-component mixture distributions by utilizing flood timescale to classify flood types in seasonally snow covered region. *Journal of Hydrology*, 574, 588–608. <https://doi.org/10.1016/J.JHYDROL.2019.04.056>
- Yin, X., & Zhou, L. (2018). Dominant modes of wintertime precipitation variability in northwest China and the association with circulation anomalies and sea surface temperature. *International Journal of Climatology*, 38(13), 4860–4874. <https://doi.org/10.1002/joc.5703>
- Yue, S., Pilon, P., & Phinney, B. (2003). Canadian streamflow trend detection: Impacts of serial and cross-correlation. *Hydrological Sciences Journal*, 48(1), 51–63. <https://doi.org/10.1623/HYSJ.48.1.51.43478>
- Yue, S., & Wang, C. Y. (2002). Applicability of prewhitening to eliminate the influence of serial correlation on the Mann-Kendall test. *Water Resources Research*, 38(6), 1068–1074. <https://doi.org/10.1029/2001WR000861>
- Zhou, Y. (2020). Exploring multidecadal changes in climate and reservoir storage for assessing nonstationarity in flood peaks and risks worldwide via an integrated frequency analysis approach. *Water Research*, 185, 116265. <https://doi.org/10.1016/J.WATRES.2020.116265>
- Zveryaev, I. I. (2006). Seasonally varying modes in long-term variability of European precipitation during the 20th century. *Journal of Geophysical Research*, 111. <https://doi.org/10.1029/2005JD006821>